

# Observations of Cold Dust in Nearby Elliptical Galaxies

Lerothodi L. Leeuw,<sup>1</sup> Anne E. Sansom,<sup>2</sup> E. Ian Robson,<sup>3</sup> Martin Haas,<sup>4</sup>  
and Nario Kuno<sup>5</sup>

## ABSTRACT

Spectral energy distribution (SED) analyses, that include new millimeter (mm) to far-infrared (FIR) observations, obtained with continuum instruments on the Nobeyama and James Clerk Maxwell Telescopes and *Infrared Space Observatory* (*ISO*), are presented for seven, nearby ( $< 45$  Mpc) FIR-bright elliptical galaxies. These are analyzed together with archival FIR and short-wave radio data obtained from the NASA/IPAC Extragalactic Database (NED). The radio to infrared SEDs are best fit by power-law plus greybody models of dust residing in the central galactic regions within 2.4 kpc diameter and with temperatures between  $\sim 21$  and 28 K, emissivity index  $\simeq 2$ , and masses from  $\sim 1.6$  to  $19 \times 10^5 M_{\odot}$ . The emissivity index is consistent with dust constituting amorphous silicate and carbonaceous grains previously modeled for stellar-heated dust observed in the Galaxy and other nearby extragalactic sources. Using updated dust absorption coefficients for this type of dust, dust masses are estimated that are similar to those determined from earlier FIR data alone, even though the latter results implied hotter dust temperatures. Fluxes and masses that are consistent with the new FIR and submm data are estimated for dust cooler than 20 K within the central galactic regions. Tighter physical constraints for such cold, diffuse dust (if it exists) with *low* surface brightness, will need sensitive FIR-submm observations with the *Spitzer Space Telescope*, SCUBA2, or ALMA.

---

<sup>1</sup> Ritter Astrophysical Research Center, University of Toledo, Mail Stop 113, 2801 West Bancroft Street, Toledo, OH 43624; leeuw@astro1.panet.utoledo.edu.

<sup>2</sup> Centre for Astrophysics, University of Central Lancashire, Preston PR1 2HE, United Kingdom; aesansom@uclan.ac.uk.

<sup>3</sup> Astronomy Technology Centre, Royal Observatory, Blackford Hill, Edinburgh EH9 3HJ, United Kingdom; eir@roe.ac.uk.

<sup>4</sup> Astronomisches Institut, Ruhr-Universität Bochum, 44780 Bochum, Germany; haas@astro.ruhr-uni-bochum.de.

<sup>5</sup> Nobeyama Radio Observatory, Minamimaki, Minamisaku, Nagano 384-1305, Japan; kuno@nro.nao.ac.jp.

*Subject headings:* galaxies: elliptical and lenticular, cD — galaxies: ISM — galaxies: photometry — infrared: galaxies — radio continuum: galaxies — submillimeter

## 1. Introduction

Optical-absorption patches, lanes, and filaments of dust have been seen in 50 to 80% of nearby bright elliptical galaxies (e.g. van Dokkum & Franx 1995). Observations at a range of other wavelengths have also revealed unexpected amounts of gas and dust in these galaxies (e.g. Roberts et al. 1991; Goudfrooij et al. 1994). In some objects, the dust masses estimated from optical extinction studies are a magnitude lower than masses implied by the *IRAS* far-infrared (FIR) fluxes, suggesting that ellipticals may contain diffusely distributed dust not detected or properly accounted for in optical observations (e.g. Goudfrooij & de Jong 1995). The dust would add another degeneracy to age-metallicity degeneracies, further complicating the interpretations of broadband colors (e.g. Wise & Silva 1996). Attenuation by the dust would also produce effects similar to the expected kinematical signature of a dark matter halo, and thus provide an alternative explanation for the usual stellar kinematical evidence for dark matter haloes around elliptical galaxies (e.g. Baes & Dejonghe 2002). Therefore, constraining the physical properties of the dust is very crucial.

The *IRAS* FIR beams were  $> 1'$  and sampled only the spectrum of dust at temperatures  $> 25$  K, providing poor constraints on the dust distribution and emission from dust  $< 25$  K. Using the previous generation submm detector, UKT14 (Duncan et al. 1990), Knapp & Patten (1991) did not detect any submm dust emission from their sample of radio galaxies, that included many *IRAS*-detected ellipticals. They assumed dust temperatures of  $\sim 18$  K, as estimated for Galactic dust (e.g. Reach et al. 1995); and, boosted by the lower dust temperatures, they inferred large dust contents of  $\sim 10^6 - 10^8 M_{\odot}$ , i.e. as found in luminous spiral galaxies. Millimeter and submm continuum emission was subsequently detected from a sample of early-type galaxies by Fich & Hodge (1993) (also using UKT14). Results from these data showed that dust masses in early-type galaxies were an order of magnitude lower than seen in spirals. In a recent review of cold gas in elliptical galaxies, Knapp (1999) concluded that field ellipticals contain about 0.01 to 0.1 of the interstellar matter content of spiral galaxies of similar luminosity. Because of the dust's relative paucity, detecting its total content in ellipticals is much harder.

A re-examination of the *IRAS* detection rate and fluxes by Bregman et al. (1998)

showed that most *IRAS* detections of early-type galaxies were near the  $3\sigma$  level, with only about 12% of the galaxies in their sample having been detected above the 98% confidence level. This showed that although dust might be present in a number of early-type galaxies, a record of good FIR fluxes, that were crucial for constraining dust properties in ellipticals, existed for only a few early-type galaxies. Recent, extensive work by Temi et al. (2004) added *ISO* archival data for 39 giant elliptical galaxies to the FIR data record of ellipticals and is expected to be complemented by new FIR data from the recently launched *Spitzer Space Telescope*.

This paper extends the previous FIR to mm studies of early-type galaxies, exploiting newer, sensitive instruments, by exploring whether 2 mm to  $450\ \mu\text{m}$  data obtained with NOBA and SCUBA [which is 100 times more sensitive than UKT14 (Holland et al. 1999)], can reveal any dust component  $< 20\ \text{K}$  and constrain the total content in selected nearby field ellipticals. The mm to submm measurements from NOBA and SCUBA, which are obtained respectively at the Nobeyama<sup>1</sup> and James Clerk Maxwell Telescopes (JCMT),<sup>2</sup> are used together with archival 60 and  $100\ \mu\text{m}$  *IRAS*-NED<sup>3</sup> and new 60 to  $200\ \mu\text{m}$  *ISO* data,<sup>4</sup> with the aim of tightening physical properties of cold dust that emits in these wavebands. The thermal emission fluxes from the mm to FIR continuum are analyzed together with some archival radio data, obtained from NED, to account for any non-thermal, high-frequency radio synchrotron contribution to the cold dust spectrum. Some *IRAS* data were re-processed using HIRES- and SCANPI routines at the NASA/IPAC Center and used to check the data for any FIR source confusion or contamination.

---

<sup>1</sup>The Nobeyama Telescope is operated by the Nobeyama Radio Observatory (NRO), which is a branch of the National Astronomical Observatory of Japan.

<sup>2</sup>The JCMT is operated by the Joint Astronomy Centre on behalf of the United Kingdom Particle Physics and Astronomy Research Council (PPARC), the Netherlands Organisation for Scientific Research, and the National Research Council of Canada.

<sup>3</sup>The NASA/IPAC Extragalactic Database (NED) is operated by the Jet Propulsion Laboratory, California Institute of Technology, under contract to the National Aeronautics and Space Administration.

<sup>4</sup>Based on observations with the Infrared Space Observatory ISO, an ESA project with instruments funded by ESA Member States (especially the PI countries: France, Germany, the Netherlands and the United Kingdom) and with the participation of ISAS and NASA.

## 2. Source Selection, Far-infrared Data, and Submm-to-mm Observations

The elliptical galaxies selected for submm-to-mm observations had *IRAS*-detected 60 and 100  $\mu\text{m}$  emission that was thought to indicate excess dust over their optically determined dust masses (e.g. Goudfrooij et al. 1994; Wise & Silva 1996). In order to maximize the detection of expected, low-level fluxes and with the aim of spatially resolving them, the targets are relatively strong FIR emitters ( $> 100 \text{ mJy}$ ) and nearby ( $< 45 \text{ Mpc}$ ). To avoid confusing any non-thermal flux contribution to the detected thermal emission, the galaxies, apart from NGC 4374, are low-radio emitters. They include ellipticals that had inferred dust masses greater than  $\sim 10^5 M_{\odot}$  in samples by Knapp & Patten (1991); Goudfrooij & de Jong (1995); and Bregman et al. (1998).

ISOPHOT photometry observations from 60 to 200  $\mu\text{m}$  (Lemke et al. 1996) of the five galaxies NGC 3962, NGC 4374, NGC 4697, and NGC 5353/NGC 5354 were obtained from the *ISO* Data Archive (Kessler et al. 2000). They were reduced using the PHOT Interactive Analysis tool (PIA V9.1) together with the calibration data set V7.0, providing a photometric accuracy of better than 30% for faint sources (Laureijs & Klaas 1999).

NGC 3962, NGC 4374 and NGC 4697 were observed in chopped mode (ISOPHOT AOT 22) and NGC 5353/5354 in sparse mapping (ISOPHOT AOT 37/39). The data reduction included correction for the electronics’ non-linearity, removal of data sections contaminated by cosmic particle events (also known as deglitching), and correction for signal dependence on the reset interval time. For the chopped observations, the data reduction also included correction for transient effects using the so-called “pattern-analysis” method. As a cross check on this technique, a Fourier-analysis method was also applied as described in detail by Haas et al. (2000), yielding similar results to within 10%. Further reduction included the calibration of the detector responsivity and its changes, performed using associated measurements of the thermal fine calibration source on board.

All *ISO* source fluxes were corrected for aperture size assuming an unresolved point source, since on the ISOPHOT C100 array (which has  $3 \times 3$  pixels of diameters  $46''$ ) no indication for any significant, extended 60-to-100  $\mu\text{m}$  flux was found beyond the pixel resolution. The photometry in the 60-to-100  $\mu\text{m}$  wavebands was derived from the  $46''$ , central-C100 pixel pointed at the source. For the chopped 170 and 200  $\mu\text{m}$  observations, where the sources were centered on the  $2 \times 2$  pixel array, the photometry was derived from the whole array ( $180''$ ), as in that case the source flux was measured by all four pixels (see, e.g., top-left panel of Figure 1). Slightly different flux extraction was required for the 180  $\mu\text{m}$  observations of the companion galaxies NGC 5353 and NGC 5354, because both objects were detected by this array simultaneously (see details below).

The top panels in Figure 1 show that the galaxies NGC 5353 and NGC 5354 are only about  $70''$  apart, with the latter being in the north. This is sufficiently close for the two galaxies to be covered by the ISOPHOT C100 and C200 arrays, that have  $3 \times 3$  and  $2 \times 2$  pixels of size  $46''$  and  $92''$  each, respectively, and to allow the galaxies to be resolved on the C100 array. As shown on the left panels in Figure 1, NGC 5353 and NGC 5354 were respectively observed exactly with the center and corner pixels of the C100 array, ensuring that the galaxies would be clearly resolved from each other on this array. Those C100 pixels which are not centered on the two sources show some low-level flux (bottom-left histogram of Figure 1), which stems from the wings of the point spread function, primarily of the central source. The same applies for the observations at  $60 \mu\text{m}$ . The right panels of Figure 1 show that at  $180 \mu\text{m}$  NGC 5353 is centered on the  $2 \times 2$  pixels of C200 array, so that its flux is distributed over all four pixels, and NGC 5354 is located on the corner pixel containing most of its flux. In order to separately extract the  $180 \mu\text{m}$  fluxes of the two galaxies on the C200 array, two point sources were fitted to the measured fluxes – one was centered on the array and the other located almost exactly on a corner pixel, corresponding to the C100 array positions of NGC 5353 and NGC 5354 respectively. This paper exploits the new *ISO* data of NGC 5354 and NGC 5353 and deals with these companion galaxies as individual FIR sources. For the first time ever (see details about the corresponding *IRAS* measurements below), the two galaxies are resolved from each other at 60 and  $100 \mu\text{m}$ , and their fluxes are separately extracted at  $180 \mu\text{m}$ . It is noted that Temi et al. (2004) did not resolve the pair NGC 5354 and NGC 5353 in their recent, extensive analysis of the same *ISO* data as presented here.

Photometric observations in the submm were obtained with SCUBA on various nights from 2001 January to 2002 February. The camera was simultaneously operated with the central bolometers of the short-wave array at  $450 \mu\text{m}$  and the long-wave array at  $850 \mu\text{m}$ . The photometry employed a 9-point jiggle pattern in a  $3 \times 3$  grid of  $2''$ , and standard SCUBA data reduction was undertaken (e.g. Leeuw et al. 2000). The fluxes were calibrated using instrumental gains determined from photometry observations of planets and, when planets were not available, the JCMT secondary calibrators (Sandell 1998; Jenness et al. 2002).

On 2002 March 4, the ellipticals NGC 4374, NGC 4697, and NGC 5353 were scan-mapped at 2 mm with the NOBA bolometer array attached to the Nobeyama-45-m Telescope. During the telescope allocation for this study, only three objects were observed because there was only a limited spell of good weather. The typical sky opacity ( $\tau$ ) during the observation was 0.12, measured using skydips. Exposure times were  $\sim 90$  minutes per galaxy, raster-scanning across each target to obtain maps of  $1 \times 1$  arcminutes. Primary flux calibration observations were obtained on Saturn and secondary calibration on 3C273 and 3C279. The expected flux for Saturn was obtained from the JCMT planetary flux program

and those for 3C273 and 3C279 were boot-strapped from JCMT monitoring observations. There was no indication of extended emission beyond the NOBA-12'' beam (FWHM) at 2 mm. The resultant FIR to mm flux estimates and upper limits are presented in Table 1.

There is a discrepancy between the *IRAS* and *ISO* fluxes of NGC 5353 and NGC 5354; this is because, on *IRAS* scans, NGC 5354 was not resolved from NGC 5353, and only the combined flux of the galaxy pair was listed in the *IRAS* point source catalog (PSC). Compared with the combined *ISO* fluxes of the galaxies, the *IRAS* PSC flux is much smaller, i.e., only about 50%. The baseline determined by the *IRAS* PSC algorithm generally uses an unresolved point source filter, so that for a moderately extended source like the pair NGC 5353/5354 the baseline is set at the level of the extended emission, i.e., too high, resulting in too a low source flux. A similar trend of too low *IRAS* PSC fluxes was found for 12 moderately resolved spiral galaxies (Bendo et al. 2002, their section 4.1.3). An examination of the SCANPI-processed-*IRAS* scans around NGC 5353 shows that the low *IRAS* fluxes might be caused by a poor baseline determination on the pair NGC 5353/5354, plus some extended flux contribution from another 4' nearby source. A visual inspection of the scans and baselines for the pair gives  $F(60\ \mu\text{m}) = 0.45\ \text{Jy}$  and  $F(100\ \mu\text{m}) = 1.9\ \text{Jy}$ , which comes close to the *ISO* values of  $F(60\ \mu\text{m}) = 0.6\ \text{Jy}$  and  $F(90\ \mu\text{m}) = 1.95\ \text{Jy}$ . This leads to a conclusion that the 60 and 100  $\mu\text{m}$  *ISO* fluxes of NGC 5353 and NGC 5354 in this paper are correct and the newly determined fluxes are used in the spectral energy distribution (SED) analyses below. It is interesting that despite the decomposition of the 180 $\mu\text{m}$  fluxes, the SEDs of NGC 5353 and NGC 5354 are not much different from those of the other sources presented in this paper (see Section 4 below).

### 3. Beam Sizes and Source Fluxes and Extents

The fluxes presented here (see Table 1) come from single-pointing observations obtained with beams that vary in size. The *IRAS* 60 and 100  $\mu\text{m}$  are  $\sim 120'' - 240''$ , *ISO* 170 to 200  $\mu\text{m}$  180'' (except 92'' for NGC 5353 and NGC 5354), *ISO* 60 to 100  $\mu\text{m}$   $\sim 46''$ , SCUBA 850  $\mu\text{m}$   $\sim 16''$ , NOBA 2 mm  $\sim 12''$ , and SCUBA 450  $\mu\text{m}$   $\sim 9''$  (FWHM in all cases, except the 180'' for the *ISO* 170 to 200  $\mu\text{m}$  is  $2\times$  FWHM). Therefore, if the FIR to submm emission from the targets is as extended as the galaxies' effective radii, i.e. 14'' to 72'' (see Table 2), then for each object, the fluxes from the respective instruments will come from different galactic regions corresponding to the sampling beam sizes.

Mindful of this and for reasons noted below, the SED analyses here assume that all the fluxes come from predominantly unresolved, central regions of the galaxies, whose extent is less than the employed mm to *ISO*-100  $\mu\text{m}$  beams, i.e.  $< 8''$  to  $< 46''$ , or roughly  $< 1\ \text{kpc}$

to  $<6$  kpc galactic scales. As noted earlier, at least 50% of nearby bright ellipticals have dust features that manifest absorbing optical light within areas of such nuclear regions. Some ellipticals also show a compact nucleus associated with radio emission in some of these galaxies (e.g. Bower et al. 1997). The submm emission from these cores is expected to be the high frequency extrapolation of synchrotron radiation that is responsible for the radio source. Leeuw et al. (2002) showed that this emission can be comparable to the total submm flux from low level dust emission, and therefore needs to be accounted for when analyzing any possible submm re-radiation from dust, especially in unresolved sources with active nuclei.

The assumption that the FIR to submm emission comes from a dominant unresolved region in the presented observations is made following NOBA-, SCUBA- and ISOPHOT-mapping results of three of the galaxies studied here, i.e. NGC 4374, NGC 5353, and NGC 5354. First, the SCUBA mapping observations by Leeuw et al. (2000) showed that the  $850\ \mu\text{m}$  continuum from this object was unresolved, constraining the emitting source by the SCUBA-850 resolution to  $< 16''$ . Second, the NOBA mapping results of NGC 4374 and NGC 5353 constrain the 2 mm-emission from these galaxies by the NOBA resolution to  $< 12''$ . Similarly, the ISOPHOT mapping results constrain the  $100\ \mu\text{m}$ -emission from NGC 5353 and NGC 5354 to  $< 46''$ . Consistent with the above assumption, the parameter results of the SED model fitting require that the emitting-greybody sources in all the studied ellipticals are less than about  $9''$  (see below). This is true for single-temperature-greybody sources with the standard dust emissivity indices from 1 to 2. However, in the case the SED model fitting is computed for two-(or-more)-temperature-greybody sources (Leeuw et al. 2002), where one of the temperatures is considerably lower than results presented in this paper, larger emitting regions for the coldest dust could be implied.

Removing the assumption that the emitting regions detected here are unresolved could have some consequence on the fitting and derived parameters. In particular, if the detected FIR to mm emission is extended, the larger FIR beams could include emission from outside the very central regions ( $\sim 8''$  to  $16''$ ) sampled by the mm and submm beams and imply that the mm and submm fluxes are undersampled relative to the FIR data in the SED fits. The SED fitting to the “undersampled”, lower submm fluxes ( $F_\nu$  or  $S_\nu$  below) would (a) require higher emissivity index ( $\beta$ ) values to match the slope at the Raleigh Jeans tail, (b) imply smaller emitting region or scaling factor ( $\Omega$ ) values (from Equation 1,  $F_\nu \propto \Omega$ ), and (c) yield lower dust mass determinations (from Equation 3,  $M_d \propto S_\nu$ ) than would be estimated with the higher submm fluxes.

#### 4. Decomposing the SED

To model the radio to infrared SED, a combination of a power-law (non-thermal radio emission from the galaxy’s nucleus) plus greybody (re-processed emission from dust) was used. The composite model flux is

$$F_\nu = C\nu^\alpha + \Omega B_\nu(T)[1 - \exp(-(\frac{\lambda_o}{\lambda})^\beta)], \quad (1)$$

where  $C$  is the normalization for the power-law component,  $\alpha$  the power-law spectral slope with  $F_\nu \propto \nu^\alpha$ ,  $\Omega$  the solid angle for the greybody component,  $B_\nu(T)$  the Planck function at temperature  $T$ ,  $\lambda_o$  the wavelength at which the optical depth is unity and  $\beta$  the emissivity index of the grains. Due to the limited frequency sampling in the data, the temperature  $T$ , and its uncertainty are the only key parameters that are statistically determined in Equation 1. Therefore, in fitting Equation 1, the factors  $C$  and  $\Omega$  were normalized to the data, the temperature was allowed to vary and statistically computed, and the power-law index  $\alpha$  and emission parameters  $\lambda_o$  and  $\beta$  were fixed and adopted, as described below.

The normalizing factors  $C$  and  $\Omega$  were obtained by forcing the model flux to agree with the core-radio (1.4 and 5 GHz) and FIR (60 and 100  $\mu\text{m}$ ) fluxes respectively, since the two components dominate in these different wavebands; and, the best fitting values for the temperatures and their uncertainties were determined by minimizing  $\chi^2$  for preset values of  $\beta = 1, 1.5, 1.8$ , and 2 in Equation 1. Following Leeuw et al. (2000) and references therein,  $\lambda_o = 7.9 \mu\text{m}$  and  $\alpha = -0.25$  were fixed and used on fits for all objects but NGC 2986 and NGC 5353, for which, from examinations of their fits by eye, the mm and submm data clearly required steeper power-law slopes of  $\alpha = -0.5$  and  $-0.3$  respectively (cf. Table 2).

The lowest  $\chi^2$ ’s, i.e., best fits, were obtained with  $\beta = 2$ , and the worst with  $\beta = 1$ . In general, the fits became worse and yielded slightly higher temperatures with decreasing  $\beta$ . Relative to values obtained with  $\beta = 2$ , the temperatures obtained with  $\beta = 1.8$  and 1.5 were greater by  $T \sim 2$  and  $\sim 4$  K, respectively. Table 2 lists the temperatures and  $\chi^2$ ’s for  $\beta = 1.5$ , as a demonstration of the higher temperatures and poorer fits with  $\beta < 2$ . The table also shows that while values of  $\beta = 2$  looks best, there is not a lot to choose between that and values of  $\beta = 1.5$ , indicating the degree of uncertainty in the fits. For temperature values determined here, a choice of  $\beta$  primarily affects the SEDs longward of 100  $\mu\text{m}$ , so that for NGC 3962 and NGC 5354, for which there are only flux upper limits or no FIR to submm data points longward of 100  $\mu\text{m}$ , the  $\beta$  providing the best fit (i.e., lowest  $\chi^2$ ) for these objects cannot be discriminated. For NGC 4374, the differences in 60 and 100  $\mu\text{m}$  fluxes are the dominant contributor to the  $\chi^2$ ; and therefore, the  $\chi^2$  with different  $\beta$ ’s for this object are about the same.

Mindful of the fitting uncertainties, the general deduction in this paper is that the re-



duced  $\chi^2$ 's that are listed in Table 2 analysis demonstrate that single temperature greybodies with  $\beta = 2$  produced reasonable SEDs fits for the objects presented here (see also Section 4.2 below). For NGC 3962 and NGC 4697 that appear to have better  $\beta = 1.5$ ,  $\chi^2$  than  $\beta = 2$ ,  $\chi^2$ , submm upper limits not included in the  $\chi^2$  determination fall below the  $\beta = 1.5$  model plots but are consistent with the  $\beta = 2$  plots. Therefore, greybodies with temperatures obtained from these  $\beta = 2$  fits are adopted in this paper. They are plotted as dotted lines in Figure 2 and their derived parameters listed in Table 2. The power-law plus greybody model is plotted as solid or dashed lines (see Figure 2), respectively for power-law indices of NGC 4374, that was determined from linear regression fits by Leeuw et al. (2000), and of the other galaxies, that have been fixed following the results of NGC 4374 as described above. New mm-submm observations obtained with the Nobeyama Telescope and SCUBA are marked by open squares and circles respectively. New FIR data from *ISO* are indicated by asterisks. Other infrared 100 and 60 $\mu\text{m}$  data in the figures are from *IRAS*, which together with all radio data were obtained from NED. The downward arrows indicate 3- $\sigma$  upper limits.

#### 4.1. Limitations of Data and SEDs for Individual Galaxies

Because of the submm and mm faintness of sources presented and the limited sensitivity of instruments used, about half of the submm and mm data points are upper limits. Therefore, some galaxies in the sample have little or incomplete mm to FIR observational data sets to allow a model fitting to the SEDs with the full range of variables that could be considered as free parameters in Equation 1. Also, some *ISO* data duplicate the *IRAS* measurements at 60 and 100  $\mu\text{m}$ , such that, even when the number of free parameters to fit to the data are restricted as described above (see Section 4), a few of the galaxies are still left with too few data and too many free parameters in the fitting process.

Specifically, NGC 2986 has only two photometric data points and three upper limits in the mm to FIR regime. Therefore, no reduced  $\chi^2$  was computed for this object. The dust temperature obtained can be thought of as derived from the 60 to 100  $\mu\text{m}$  flux ratio, as commonly derived for objects with only *IRAS* data (e.g. Goudfrooij & de Jong 1995). A tentative composite plot for this object is displayed in Figure 2 to demonstrate the consistency of the mm-submm upper limits and FIR data with the model fit. Similarly, a tentative dust mass for this object is computed as described for the other objects below and listed in Table 2.

It is noted that NGC 3156 has limited number of data points. However, the three points this galaxy has in the FIR to submm region are sufficient for making the required fit to the temperature and normalisation of its thermal spectrum. It is also noted that NGC 4697 has

only 3 upper limits in the cm-submm region. However, this object has a very good sampling of points around the peak of the thermal spectrum; and so, for NGC 4697, the upper limits in mm-submm region are not needed or used to provide any constraints and are plotted primarily to show that these data are consistent with the fit.

Currently only limited data is available for fitting the power-law spectrum in the region from 1.4 to 5 GHz. As noted earlier, the power-law index is therefore fixed at  $-0.25$  for all the galaxies but for NGC 2986 and NGC 5353, where it is estimated as  $-0.50$  and  $-0.30$  respectively. Fixing the index follows fits of NGC 4374 in earlier work (Leeuw et al. 2000), since this source has the needed points from 1.4 to 5 GHz. Commissioning of high frequency radio instruments such as the Green Bank Telescope should allow data in these wavebands to be obtained for other ellipticals in the future, enabling more reliable correction of non-thermal contribution to the mm-FIR thermal flux. As noted earlier, the  $C$  parameter normalizes the power-law component of the model to the 1.4 and 5 GHz data, for either detected points or upper limits, depending on the presently scant availability of needed data in literature and archives. This normalization is done well aware that it is less reliable in the cases such as for NGC 3156 and NGC 4697, where only 5 GHz upper limits are currently available.

#### 4.2. A Second Dust Component with $T < 20$ K?

Spectral energy distribution analyses by Dunne & Eales (2001) and Klaas (et al. 2001), among others, have demonstrated evidence for thermal emission with at least two temperature components and an emissivity index of 2. This was for samples of bright *IRAS* and ultra-luminous infrared galaxies and was deduced not only from rigorous fitting results but also physical considerations. The presence of very cold dust has also been suggested in some individual sources, e.g. the peculiar dwarf elliptical galaxy NGC 205 (Haas 1998) and the merger-remnant elliptical galaxy NGC 5128 (Leeuw et al. 2002).

Following the investigations by Dunne & Eales (2001) and Klaas (et al. 2001), the FIR to submm data are also fit with two-component greybodies to test whether such greybodies, including those with components of temperatures less than 20 K (see Figure 3), produce better fits than single-temperature models. That the single-temperature greybodies alone do not fit both FIR and submm data simultaneously may indicate that there is a second very cold (i.e.,  $< 20$  K) dust component required. The data longward of  $100 \mu\text{m}$ , as newly available for this paper, can sample fluxes from dust with temperatures not only in the *IRAS* range of  $T \sim 20$  to 100 K, but also less than 20 K. However, the current data coverage is too sparse in wavelength space and in some cases the detections have relatively large uncertainties or only flux upper limits are available. Therefore, it is not possible to *reliably* determine the exact

decompositions of the 6 to 20 K (very cold) and 20 to 40 K (cold) components or *securely* discriminate whether two-temperature fits are better than single-temperature ones for all galaxies.

For now, the SEDs for which there were at least three data points from 100 to 850  $\mu\text{m}$  allow an eyeball fit that is useful for estimating the flux upper limit for the very cold dust temperatures component that is consistent with the data. In this regard and to facilitate comparison with fits from Equation 1, a two-temperature component greybody of the form

$$F_\nu = C\nu^\alpha + \Omega[B_\nu(T_1) + B_\nu(T_2)][1 - \exp(-(\frac{\lambda_o}{\lambda})^\beta)], \quad (2)$$

where the parameters are as in Equation 1, was fit to the FIR-submm data of NGC 3962, NGC 4374, NGC 4697 and NGC 5353 (see Figure 3). The modelled-flux sums of two-temperature greybodies are normalized to detected-FIR or -submm fluxes, and it is assumed that the greybodies for respective galaxies have the same solid angles and emissivity indices as obtained from Equation 1 and listed in Table 2.

Figure 3 exhibits the composite and individual greybodies that constitute the composites by dashed-three-dotted and purely dotted lines, respectively. Because it is the sum of the two components that are normalized to the data, curves of the composite and individual greybodies respectively fall on and below the submm data. For NGC 3962, the observed 850  $\mu\text{m}$ , 3- $\sigma$  limit of 0.009 Jy is fit by 12 and 24 K greybodies with modelled 850  $\mu\text{m}$  fluxes of 0.0012 and 0.0078 Jy, respectively; for NGC 4374, the observed 450  $\mu\text{m}$  flux of 0.110 Jy is fit by 12 and 31 K greybodies with modelled 450  $\mu\text{m}$  fluxes of 0.086 and 0.034 Jy, respectively; for NGC 4697, the observed 850  $\mu\text{m}$ , 3- $\sigma$  limit of 0.007 Jy is fit by 12 and 27.5 K greybodies with modelled 850  $\mu\text{m}$  fluxes of 0.009 and 0.0061 Jy, respectively; and, for NGC 5353, the observed 850  $\mu\text{m}$  flux of 0.017 Jy is fit by 9 and 27 K greybodies with modelled 850  $\mu\text{m}$  fluxes of 0.011 and 0.006 Jy, respectively. The modelled-submm fluxes of very cold dust components provide flux estimates of emission that would originate from a second dust component at the respective temperatures and may be consistent with the submm-FIR data. If there's any additional flux contribution to observed submm flux, the modelled flux from very cold dust components will scale down in proportion to the contributing flux.

Although the two-temperature model may be consistent with the data, it produced relatively high reduced  $\chi^2$  of 2, 4.6, 1.6, 2.2 respectively for NGC 3962, NGC 4374, NGC 4697, and NGC 5353 (see Table 2), showing that under the fitting criteria assumed in this paper, the single-temperature model of the form in Equation 1 fits the presented data slightly better than the two-temperature model. Following this comparison and the fact that the model fits are based on under-sampled SEDs with many upper limits, this paper cannot positively identify (or rule-out) the presence of cold dust < 20 K in the presented elliptical galaxies.

## 5. Derived Dust Parameters

The best fitting power-law plus greybody model to the radio-to-infrared SEDs constrains the dust to central galactic regions of diameters  $\sim 0.4$  to  $2.4$  kpc ( $5''$  to  $9''$ ), average dust temperatures between  $\sim 21$  and  $28$  K, and emissivity index  $\beta \simeq 2$  (see Table 2). It was noted in Section 4 that when the new submm to *ISO*-FIR data are not considered, such as in the  $\chi^2$  determinations that do not use the submm-FIR upper limits, it appears that some model fits with  $\beta = 1.5$  are as good or better than those with  $\beta = 2$  (see Table 2). However, it was also noted that for NGC 3962, NGC 4374, and NGC 4697, submm upper limits not included in the  $\chi^2$  determination fall below the  $\beta = 1.5$  model plots but are consistent with  $\beta = 2$  plots, favoring models with  $\beta = 2$  (cf. Section 4). Because the size of a dust emitter is inversely proportional to the dust emissivity index and temperature, the diameters derived for  $\beta = 2$  are upper limits for  $\beta$  that ranges for 1 to 2 and may be larger for dust with temperatures lower than plotted in Figure 2. However, such larger emitting regions would be required to emit flux levels much lower than detected in the presented observations. The dust temperatures around 20 K and emissivity index ( $\beta \approx 2$ ), especially, show that dust in ellipticals can exhibit properties similar to those in the Galaxy (cf. dust temperature of 16 to 21 K and emissivity index of 2, Reach (et al. 1995)), and probably constitute similar model-predicted amorphous silicate and carbonaceous grains (Li & Draine 2001).

Following Hildebrand (1983), the mass of emitting dust  $M_d$  can then be estimated from

$$M_d = \frac{S_\nu D^2}{k_d B(\nu, T)}, \quad (3)$$

where  $S_\nu$  is the measured flux density at frequency  $\nu$ ,  $D$  is the distance to the source,  $B(\nu, T)$  the Planck function and  $k_d = 3Q_\nu/4a\rho$  the grain mass absorption coefficient where  $a$  and  $\rho$  are respectively the grain radius and density. Recently updated values of  $k_d^{100\mu\text{m}} = 3.5 \text{ m}^2\text{kg}^{-1}$  and  $k_d^{60\mu\text{m}} = 10.62 \text{ m}^2\text{kg}^{-1}$  (Li & Draine 2001), for Galactic-like dust (cf. above), are assumed, yielding dust masses that range from  $\sim 1.6 \times 10^5 M_\odot$  to  $1.9 \times 10^6 M_\odot$  (see Table 2).

These dust masses are of similar range as determined in the FIR studies by Roberts et al. (1991) and Goudfrooij & de Jong (1995), even though those workers used  $k_d$  values that are typical for dust with emissivity index less than 1.5 (e.g. Hildebrand 1983; Draine 1990) and about 3 times less than the values used here. The difference in the employed  $k_d$  values is balanced by the fact that dust temperatures derived here are slightly cooler than when estimated from FIR data alone (c.f. Roberts et al. 1991; Goudfrooij & de Jong 1995; Bregman et al. 1998), leading to lower values of  $B(\nu, T)$  for this work and the similarity in the dust mass estimates. One advantage of the current study is that, instead of assuming the dust emissivity index and estimating the dust temperatures from the *IRAS* 60  $\mu\text{m}$  and 100  $\mu\text{m}$

flux ratio (c.f. Roberts et al. 1991; Goudfrooij & de Jong 1995), the emissivity index and dust temperatures have been constrained by new FIR and submm to mm data that extend to longer wavelengths than earlier *IRAS* observations and better sample the Rayleigh-Jeans tail of the cold dust thermal spectrum. As noted earlier, the resulting constraints suggest that dust in ellipticals has similar properties as Galactic dust.

Derived parameters for NGC 2986 have relatively high uncertainties that are propagated from the *IRAS* and SCUBA data. *IRAS* data that were re-processed with HIREs and SCANPI routines at the NASA/IPAC Center indicate that this source’s *IRAS* flux is probably contaminated by a foreground or background object.

For the two galaxies NGC 3962 and NGC 4374, for which the respective  $10^{4.66}M_{\odot}$  and  $10^{4.54}M_{\odot}$  dust masses estimated from optical-extinction studies are available (Goudfrooij & de Jong 1995), the dust content determined here is about a magnitude larger than that determined from the optical studies of ellipticals, as observed by Goudfrooij & de Jong (1995) and Wise & Silva (1996). Both authors proposed that a diffusely distributed dust component not properly accounted for in the optical studies may be responsible for the extra dust mass determined in the infrared. The diffuse dust would probably be heated by a stellar radiation field that is more dilute than in the central regions and thus be relatively cold. This is withstanding the fact the dust can also be heated by the collision with electrons in the hot gas, with a contribution of the same order of the photon heating even at large radii (Temi et al. 2003). The data presented here are consistent with emission from dust marginally warmer than that seen in some FIR-bright, nearby spiral galaxies (e.g. Dunne & Eales 2001), and allow flux and dust-mass that are consistent with the data to be estimated for dust cooler than 20 K (see below) within inner galactic regions.

### 5.1. Masses for Dust with $T < 20$ K

As above, the mass  $M_d$  of FIR-to-submm emitting dust with temperature  $< 20$  K is determined using Equation 3; and, for the two-temperature dust fitting results, assuming values of  $k_d^{450\mu\text{m}} = 0.157 \text{ m}^2\text{kg}^{-1}$  and  $k_d^{850\mu\text{m}} = 0.050 \text{ m}^2\text{kg}^{-1}$  (Li & Draine 2001). For (a) NGC 5353,  $T=9$  K and  $S_{\nu}^{850\mu\text{m}} = 0.011$  Jy yield  $1.61 \times 10^4 M_{\odot}$ ; (b) NGC 4697,  $T=12$  K and  $S_{\nu}^{850\mu\text{m}} = 0.00087$  Jy yield  $8.31 \times 10^4 M_{\odot}$ ; (c) NGC 4374,  $T=12$  K and  $S_{\nu}^{450\mu\text{m}} = 0.086$  Jy yield  $6.87 \times 10^5 M_{\odot}$ ; and (d) NGC 3962,  $T=12$  K and  $S_{\nu}^{850\mu\text{m}} = 0.0012$  Jy yield  $2.71 \times 10^5 M_{\odot}$ . The fluxes used assume the only contribution to the detections is the “very cold” and “cold” dust, which may not be the case.

The 12 K dust mass estimate for NGC 4374 is of the same order as the warmer 28 K dust

mass determined for this galaxy. Therefore, if the  $450\ \mu\text{m}$  flux for this object is primarily from very cold dust, this component could be as significant as that from the 28 K dust. For this to be the case, the high-frequency, non-thermal power law would have to turn-over or cut-off before the  $450\ \mu\text{m}$  flux. The 12 K dust mass estimate for NGC 3962 is also of the same order as the warmer 24 K dust mass determined for this galaxy. In this case, this is all that can be said because only upper limit fluxes are available in the submm and no radio observations have been made to constrain any low frequency flux origin for this galaxy. For NGC 5353 and NGC 4697, the 9 K dust mass estimate is about two orders of magnitude less than the warmer 28 K and the 12 K dust mass estimate about an order of magnitude less than the warmer 25 K dust masses determined for these galaxies, respectively. Therefore in these cases, the cooler components, though of relatively considerable mass on their own, do not appear to be as significant as the warmer components within the central galactic regions.

## 5.2. Implications of the Fitted Dust Parameters

It is very interesting that the best fitting greybody model parameters require dust emitting in the mm to FIR to be centrally concentrated and less extended than the stellar component of ellipticals. Because red giant stars lose dusty gas to the ISM, if dust in ellipticals derives from these stars, the dust and stellar spatial distributions would be expected to be co-spatial. However, assuming that the dust is indeed produced by stars, as gas cools down and falls into the potential well, distributed dust may drift toward the galactic centers and settle into a central disc. Models of centrally concentrated, distributed dust and the transfer of stellar radiation in ellipticals by Witt et al. (1992) show that dust in such geometry would not affect the observed  $r^{(1/4)}$  surface brightness law (the de Vaucouleurs profile) caused by the stellar radiation. Moreover, such a distribution of dust would produce and naturally explain the central reddening (or a color gradient that changes with radius) that is observed in elliptical galaxies and cannot be completely explained by models that consider only evolutionary stellar population synthesis and metallicities (e.g. Peletier, Valentijn, & Jameson 1990).

Recent dynamical modeling of dusty gas ejected from evolved stars in ellipticals (or cD galaxies) supports a stellar origin of the central dust clouds seen in these galaxies (Mathews & Brighenti 2003). The models show that, even after entering the hot X-ray emitting gas, rapid cooling by thermal collisions with dust grains, especially in the central regions, can be faster than the dynamical time in the galactic potential or grain sputtering time, ensuring that some dust survives even in ellipticals with X-ray emitting gas. Observations indeed show that some dust exists in ellipticals; and, as noted by Knapp (1999), the dust probably

suggests ellipticals host modest star formation.

## 6. Conclusions

The current observations have detected centrally concentrated dust in ellipticals with properties similar to those in the Galaxy (e.g. Reach et al. 1995) and other nearby FIR-bright galaxies (e.g. Dunne & Eales 2001). Single-temperature, greybody-fitting results imply the dust is slightly cooler than when estimated from FIR data alone; however, dust masses determined using updated dust absorption coefficients (Li & Draine 2001) for Galactic-type dust yield masses similar to estimates from the FIR studies (e.g. Roberts et al. 1991; Goudfrooij & de Jong 1995). Tentative determinations have been made of flux and mass estimates for dust cooler than 20 K, within the central galactic regions. Resolved submm-FIR observations show a galactic dust temperature decrease from the center to the outer regions (e.g. Leeuw et al. 2002), where the radiation field heating the dust is dilute; and in ellipticals, the colder dust is most probably cool, diffusely distributed and heated by both the dilute stellar radiation and the collision with electrons in the hot gas (Temi et al. 2003). Because of the general paucity of the dust and the observation that it may be central concentrated (see above), the direct detection of diffuse, extended dust in ellipticals is challenging. If such diffuse dust with *low* surface brightness exists, observationally constraining its physical properties may be possible with deeper SCUBA observations (especially mapping) or soon to be commissioned or built sensitive instruments like the *Spitzer Space Telescope*, SCUBA2, and ALMA.

Lerothodi L. Leeuw is supported by a NASA Grant NAG5-9376. Martin Haas is supported by the Nordrhein-Westfälische Akademie der Wissenschaften, funded by the Federal State and the Federal Republic of Germany.

## REFERENCES

- Baes, M. & Dejonghe, H. 2002, MNRAS, 335, 441
- Bendo, G. J. et al. 2002, AJ, 123, 3067
- Bower, G. A., Heckman, T. M., Wilson, A. S., & Richstone, D. O. 1997, ApJL, 483, L33
- Bregman, J. N., Snider, B. A., Grego, L., & Cox, C. V. 1998, ApJ, 499, 670
- de Vaucouleurs, G., de Vaucouleurs, A., Corwin, H. G., Buta, R. J., Paturel, G., & Fouque, P. 1992, Third Reference Catalogue of bright galaxies (RC3)
- Draine, B. T. 1990, in ASSL Vol. 161: The Interstellar Medium in Galaxies, 483–492
- Duncan, W. D., Sandell, G., Robson, E. I., Ade, P. A. R., & Griffin, M. J. 1990, MNRAS, 243, 126
- Dunne, L. & Eales, S. A. 2001, MNRAS, 327, 697
- Fich, M. & Hodge, P. 1993, ApJ, 415, 75
- Goudfrooij, P. & de Jong, T. 1995, A&A, 298, 784
- Goudfrooij, P., de Jong, T., Hansen, L., & Norgaard-Nielsen, H. U. 1994, MNRAS, 271, 833
- Haas, M., Müller, S. A. H., Chini, R., Meisenheimer, K., Klaas, U., Lemke, D., Kreysa, E., Camenzind, M. 2000, A&A, 354, 453
- Haas, M. 1998, A&A, 337, L1
- Hildebrand, R. H. 1983, QJRAS, 24, 267
- Holland, W. S. et al. 1999, MNRAS, 303, 659
- Jenness, T., Stevens, J. A., Archibald, E. N., Economou, F., Jessop, N. E., Robson, E. I. 2002, MNRAS, 336, 14
- Kessler, M. F., Müller, T. G., Arviset, C., García-Lario, P., & Prusti, T. 2000, in The ISO Handbook: Vol. 1, SAI/2000-035/Dc (ESA publications)
- Klaas, U. et al. 2001, A&A, 379, 823
- Knapp, G. R. 1999, in ASP Conf. Ser. 163: Star Formation in Early Type Galaxies, 119
- Knapp, G. R. & Patten, B. M. 1991, AJ, 101, 1609



- Laureijs, R. & Klaas, U. 1999, ISOPHOT Error Budgets V1.0, ISO Explanatory Library Document, SAI/98-091/Dc (ESA publications)
- Leeuw, L. L., Hawarden, T. G., Matthews, H. E., Robson, E. I., & Eckart, A. 2002, *ApJ*, 565, 131
- Leeuw, L. L., Sansom, A. E., & Robson, E. I. 2000, *MNRAS*, 311, 683
- Lemke, D. et al. 1996, *A&A*, 315, L64
- Li, A. & Draine, B. T. 2001, *ApJ*, 554, 778
- Mathews, W. G. & Brighenti, F. 2003, *ApJL*, 590, L5
- Peletier, R. F., Valentijn, E. A., & Jameson, R. F. 1990, *A&A*, 233, 62
- Reach, W. T. et al. 1995, *ApJ*, 451, 188
- Roberts, M. S., Hogg, D. E., Bregman, J. N., Forman, W. R., & Jones, C. 1991, *ApJS*, 75, 751
- Sandell, G. 1998, *JAC WEB pages*, 271, 75
- Temi, P., Brighenti, F., Mathews, W. G., & Bregman, J. D. 2004, *ApJS*, 151, 237
- Temi, P., Mathews, W. G., Brighenti, F., & Bregman, J. D. 2003, *ApJL*, 585, L121
- van Dokkum, P. G. & Franx, M. 1995, *AJ*, 110, 2027
- Wise, M. W. & Silva, D. R. 1996, *ApJ*, 461, 155
- Witt, A. N., Thronson, H. A., & Capuano, J. M. 1992, *ApJ*, 393, 611

Fig. 1.— The infrared Digital Sky Survey (DSS) 2 images of NGC 5353 and NGC 5354 with superposed ISOPHOT C100 (top-left panel) and C200 (top-right panel) array pointings that were used for the *ISO* observations of these galaxies. The bottom-left and -right panels show 3-D histograms of the *ISO* 100 and 180  $\mu\text{m}$  fluxes, respectively, before the individual-galaxy fluxes were corrected for aperture size (see text). For visual clarity, the histograms are oriented so that the fainter source is plotted in the foreground.

Fig. 2.— Radio to far-infrared spectral energy distributions of central regions in sample FIR-bright elliptical galaxies. The model fits include a composite power law plus greybody given by Equation 1 and they together with the data symbols are as described in the text.

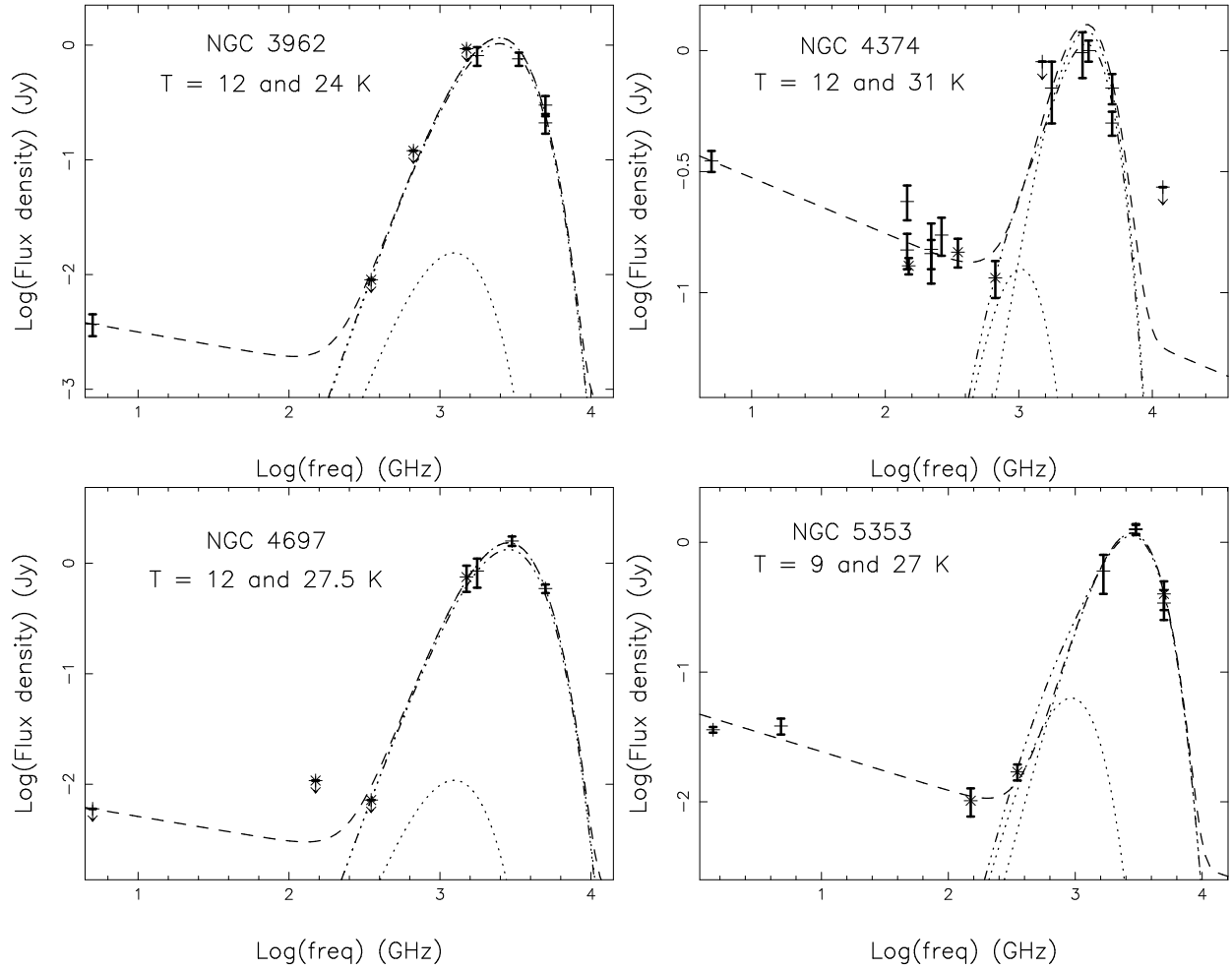


Fig. 3.— Radio to far-infrared spectral energy distributions of central regions in sample FIR-bright elliptical galaxies. The model fits are of a two-temperature greybody given by Equation 2 and they together with the data symbols are as described in the text.

Table 1. Far-infrared to mm fluxes of nearby *IRAS*-bright ellipticals.

Galaxy Name	<i>IRAS</i> 60 $\mu\text{m}$	<i>IRAS</i> 100 $\mu\text{m}$	<i>ISO</i> 60 $\mu\text{m}$	<i>ISO</i> 90 $\mu\text{m}$	<i>ISO</i> 170 $\mu\text{m}$	<i>ISO</i> 200 $\mu\text{m}$	SCUBA 450 $\mu\text{m}$	SCUBA 850 $\mu\text{m}$	NOBA 2 mm
NGC 2986	< 0.05	$0.36 \pm 0.11$	...	...	...	...	< 0.13	< .010	...
NGC 3156	$0.22 \pm 0.04$	$0.91 \pm 0.09$	...	...	...	...	< 0.06	$.006 \pm .002$	...
NGC 3962	$0.21 \pm 0.04$	< 0.98	$0.30 \pm 0.06$	$0.76 \pm 0.10$	$0.81 \pm 0.15$	< 0.91	< 0.12	< .009	...
NGC 4374	$0.50 \pm 0.06$	$0.98 \pm 0.21$	$0.70 \pm 0.10$	$1.00 \pm 0.10$	$0.70 \pm 0.20$	< 0.90	$0.12 \pm 0.02$	$.147 \pm .020$	$.129 \pm .010$
NGC 4697	$0.59 \pm 0.05$	$1.24 \pm 0.08$	$1.15 \pm 0.35^{\text{a}}$	$1.45 \pm 0.35^{\text{a}}$	$0.85 \pm 0.25$	$0.75 \pm 0.20$	...	< .007	< .010
NGC 5353	$0.32 \pm 0.06$	$1.45 \pm 0.11$	$0.40 \pm 0.10$	$1.25 \pm 0.10^{\text{b}}$	$0.60 \pm 0.20^{\text{c}}$	...	...	$.017 \pm .002$	$.011 \pm .003$
NGC 5354	$0.41 \pm 0.05$	$1.61 \pm 0.06$	$0.20 \pm 0.06$	$0.70 \pm 0.10^{\text{b}}$	$0.58 \pm 0.20^{\text{c}}$	...	...	...	...

<sup>a</sup>There is a large uncertainty in the on-board calibration measurement for this flux.

<sup>b</sup>This is an *ISO* 100  $\mu\text{m}$  filter measurement from the C100 array.

<sup>c</sup>This is an *ISO* 180  $\mu\text{m}$  filter measurement from the C200 array.

Note. — All listed fluxes are in Jansky (Jy), and errors and upper limits are respectively 1 and 3 sigma.

Table 2. Power-law plus greybody fitting results for nearby, *IRAS*-bright ellipticals.

Galaxy Name	Galaxy Type	Effect. Radii	D Mpc	P-L <sup>a</sup> index	$T_{\text{dust}}$ (K)	$\Omega_{\text{dust}}$ (ster.)	Red. $\chi^2$	$M_{\text{dust}}^{60\mu\text{m}}$ ( $\log(M_{\odot})$ )	$T_{\text{dust}}^{\text{b}}$ (K)	Red <sup>b</sup> $\chi^2$	$T_{\text{dust}}^{\text{c}}$ (K)	Red <sup>c</sup> $\chi^2$
NGC 2986	E2	36''	40.2	-0.50	$\sim 21$ ( $< 32$ )	(1.04E-9) <sup>d</sup>	N/A	( $\sim 6.28$ ) <sup>d</sup>	$\sim 23$	N/A	N/A	N/A
NGC 3156	E/SO	14''	22.3	-0.25	$24.6 \pm 0.9$	1.26E-9	0.1	$5.60 \pm .02$	28.7	3.8	N/A	N/A
NGC 3962	E1	35''	32.4	-0.25	$24.0 \pm 0.7$	1.67E-9	1.3	$5.67 \pm .02$	26.2	1.2	12/24	2.0
NGC 4374	E1	51''	20.7	-0.25	$28.1 \pm 0.9$	0.84E-9	2.5	$5.20 \pm .02$	31.5	2.8	12/31	4.6
NGC 4697	E6	72''	21.4	-0.25	$28.1 \pm 0.7$	0.94E-9	1.4	$5.60 \pm .02$	31.2	0.8	12/28	1.6
NGC 5353	E/SO	15''	45.1	-0.30	$25.3 \pm 0.9$	1.46E-9	1.0	$6.15 \pm .02$	29.2	2.5	9/27	2.2
NGC 5354	SAO: sp	18''	45.1	-0.25	$24.6 \pm 1.8$	9.00E-10	0.1	$6.16 \pm .04$	26.9	0.01	N/A	N/A

<sup>a</sup>The adopted power-law slope of  $-0.25 \pm 0.3$  for NGC 4374 is that previously fitted to the radio-to-submm data by Leeuw et al. (2000). As only limited radio to submm data are available for the other objects have, the other indices are fixed as close as the fitting reasonably permits to the value for NGC 4374.

<sup>b</sup>These values are for  $\beta = 1.5$ , for comparison to the values for  $\beta = 2$  adopted in this paper. For NGC 3962 and NGC 4697 that have better  $\beta = 1.5$ ,  $\chi^2$  than  $\beta = 2$ ,  $\chi^2$ , submm upper limits not included in the  $\chi^2$  determination fall below the  $\beta = 1.5$  model plots and favor the  $\beta = 2$  model.

<sup>c</sup>These values are for two-temperature components with  $\beta = 2.0$ , for comparison to the values for single-temperature model fits.

<sup>d</sup>The parenthesis indicate a large uncertainty due to limited data, and the dust mass is calculated from the  $100\mu\text{m}$  flux.

Note. — The galaxy types and effective radii were respectively obtained from NED and de Vaucouleurs et al. (1992)(RC3). The distances listed in column four are from earlier FIR studies (Roberts et al. 1991; Goudfrooij & de Jong 1995) to best facilitate comparison. The listed uncertainties are 1 sigma.

This figure "f1a.jpeg" is available in "jpeg" format from:

<http://arxiv.org/ps/astro-ph/0406011v1>

This figure "f1b.jpeg" is available in "jpeg" format from:

<http://arxiv.org/ps/astro-ph/0406011v1>



This figure "f1c.png" is available in "png" format from:

<http://arxiv.org/ps/astro-ph/0406011v1>

This figure "f1d.png" is available in "png" format from:

<http://arxiv.org/ps/astro-ph/0406011v1>

This figure "f2.png" is available in "png" format from:

<http://arxiv.org/ps/astro-ph/0406011v1>